Environmental Science & Technology

pubs.acs.org/est

Article

Membrane Design Criteria and Practical Viability of Pressure-Driven Distillation

Weifan Liu, Ruoyu Wang, Anthony P. Straub, and Shihong Lin*

Cite This: *Environ. Sci. Technol.* 2023, 57, 2129−2137

Read Online

ACCESS | Metrics & More | Article Recommendations | Supporting Information

ABSTRACT: Pressure-driven distillation (PD) is a novel desalination technology based on hydraulic pressure driving force and vapor transport across a hydrophobic porous membrane. In theory, PD offers near-perfect rejection for nonvolatile solutes, chlorine resistance, and the ability to decouple water and solute transport. Despite its advantages, pore wetting and the development of a reverse transmembrane temperature difference are potential critical concerns in PD, with the former compromising the salt rejection and the latter reducing or even eliminating the driving force for vapor transport. We herein present an analysis to evaluate the practical viability and membrane design principles of PD with a focus on the dependence of flux and salt rejection (SR) on membrane properties. By modeling the mass transfer in a PD process under different conditions, we arrive at two important conclusions. First, a practically detrimental reverse transmembrane temperature difference does not develop in PD under all relevant circumstances and is thus not a practical concern. Second, for a PD process to achieve an acceptable SR, the membrane pores should be at the nanometer scale with a highly uniform pore size distribution. This analysis demonstrates the practical viability of PD and provides the principles for designing robust and high-performance PD membranes.

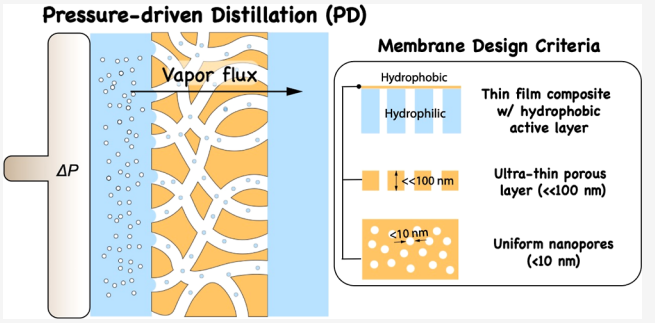

KEYWORDS: *desalination, membrane design, vapor transport, heat transfer, nanoscale, pore wetting*

INTRODUCTION

The growing global water scarcity drives technological innovations for the use of unconventional water sources.[1,2] Reverse osmosis (RO) has been proven to be a cost-effective approach for seawater desalination, brackish water desalination, and wastewater reuse.[3−5] Despite its wide applications, the current RO process based on thin-film composite polyamide (TFC-PA) membranes has intrinsic limitations.

First, despite its exceptional rejection of salts, commercial TFC-PA membranes perform poorly in rejecting small neutral solutes.[6] This weakness of TFC-PA membranes leads to insufficient removal of boron (in seawater desalination) or disinfection byproducts (in wastewater reuse) by a single-pass RO, thereby increasing the process complexity and cost for achieving the desired water quality.[7,8] Second, polyamide is susceptible to chemical degradation by strong oxidants. Therefore, biofouling control of the TFC-PA membrane cannot rely on the most cost-effective and widely adopted chlorination method.[9,10] Last, TFC-PA membranes are also constrained by the well-known permeability−selectivity trade-off, that is, increases in water permeability typically result in compromised salt rejection (SR).[11−13]

Pressure-driven distillation (PD), also known as vapor gap RO, is a conceptually novel process with the theoretical potential to overcome the challenges of TFC-PA membranes. In PD, a porous hydrophobic membrane with nanoscale pores physically separates the saline feed solution and the distillate (Figure 1A). With a sufficiently high hydraulic pressure applied to the feed solution, water evaporates from the feed solution, transports across the porous membrane down the partial vapor pressure gradient, and condenses to become the distillate.[14] PD resembles RO in using hydraulic pressure as the macroscopic driving force and resembles membrane distillation (MD) in membrane characteristics (i.e., hydrophobic porous membrane) and microscopic mass transport mechanism.[15]

The fundamental driving force of PD can be interpreted from both thermodynamic and physical perspectives. From a thermodynamic view, pressurizing the feed solution increases its chemical potential and thereby creates a trans-membrane chemical potential difference, just like in RO (see Section S1).[16,17] From a physical perspective, pressurizing the feed solution against nanoscale hydrophobic pores bends the liquid−air interface to form a convex meniscus in accordance

Received: October 21, 2022
Revised: January 11, 2023
Accepted: January 12, 2023
Published: January 24, 2023

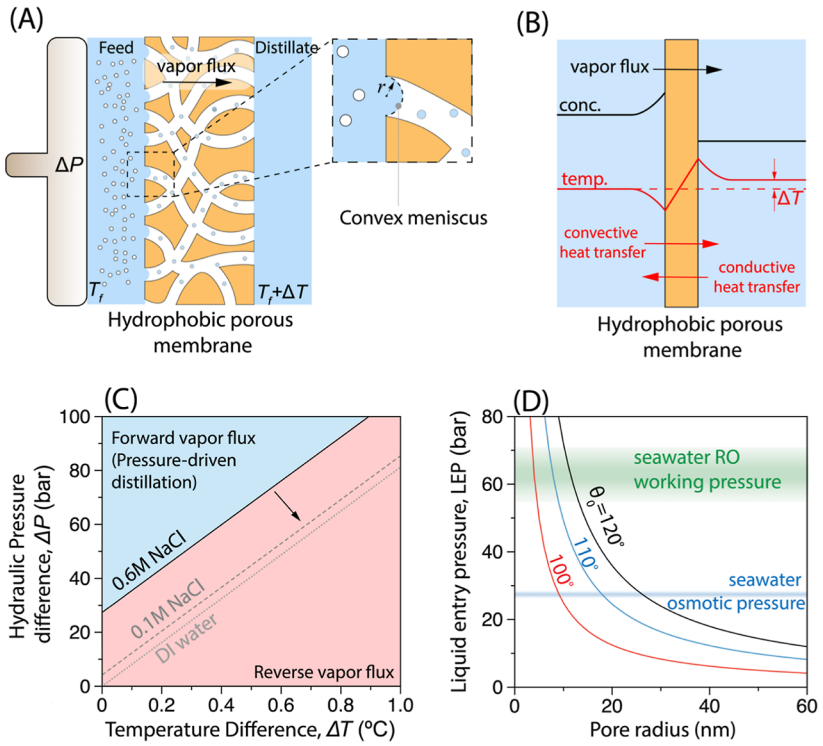

Figure 1. (A) Illustration of the working principle of PD. The pressure on the feed stream creates a convex meniscus that elevates the saturated vapor pressure of the solution. (B) Illustration of concentration profile (black solid curve), temperature profile (red solid curve), vapor flux (black arrow), and heat fluxes (red arrows) in a PD process. The arrows only reflect directions but not magnitude. (C) Two regimes of driving force as determined by hydraulic pressure difference (higher in the feed) and temperature difference (higher in the distillate). The blue region represents positive driving force (from the feed to the distillate) which generates forward vapor flux. The red region represents negative driving force which generates reverse vapor flux. A useful PD process must operate in the regime of positive driving force. (D) Liquid entry pressure (LEP) as a function of pore radius for water with membranes with three different intrinsic contact angles. Seawater osmotic pressure and the working pressure for seawater RO are also provided for comparison.

with the Young−Laplace equation. The elevation of partial vapor pressure at the convex meniscus, as quantified by the Kelvin's equation, exceeds the suppression of vapor pressure by the presence of salt and creates a net vapor pressure difference across the membrane from the feed to the distillate (detailed equations are presented in the Theory section).[14]

In theory, PD has intrinsic advantages over TFC-PA membrane-based RO. The reliance on a vapor gap for solute rejection suggests that near-perfect solute rejection is attainable for nonvolatile solutes, including small neutral molecules. Moreover, near-perfect rejection can be maintained while reducing the membrane thickness to improve vapor permeability, thus overcoming the intrinsic constraint of permeability−selectivity tradeoff in TFC-PA.[18] Additionally, the many material possibilities for fabricating nanoporous hydrophobic membranes make possible the use of chlorine or other strong oxidants for biofouling control.[19−21]

Despite all the advantages, the development of PD is in its infancy with only a few previous studies on theoretical analysis of molecular-level mass transport[14] and coupon-scale, proof-of-concept experiments with low applied pressures.[14,22−24] To make PD useful for mainstream applications, including seawater desalination, technical challenges in membrane fabrication have yet to be overcome. There are, however, two important questions regarding the practical viability of PD. The first question regards whether a significant driving force can be maintained in PD in a real membrane module, which must be answered before future PD development can be justified. The second question regards the design criteria of PD membranes and specifically whether PD membranes can resist wetting and at the same time sustain a reasonable vapor flux.

The first question is motivated as following: the mass transfer in PD (i.e., evaporation, vapor transport, and condensation) carries a significant amount of latent heat, which tends to generate a temperature difference between the feed (lower) and distillate (higher), and thereby reduces or even eliminates the driving force for vapor transport. This is the reason why the single-pass water recovery in MD is limited to a few percent.[25] A previous analysis on a thermal energy-harvesting system with similarities to PD suggests that even a tiny trans-membrane temperature difference suffices to offset a large hydraulic pressure difference.[26] Therefore, unless the development of a reverse temperature difference (higher in the distillate) can be mitigated, a PD process will unlikely work due to the rapid diminishing of driving force along the module.

This analysis aims to (1) evaluate the design principle of PD membranes considering both pore nonwetting criteria and impacts of membrane properties on vapor flux and SR and (2) assess the practical viability of PD focusing on how vapor transport driving force is affected by mass and heat transfer. We first quantitatively evaluate the driving force in PD and discuss the nonwetting criteria. We then examine the dependence of vapor flux on membrane properties including thickness, pore size and its distribution, porosity, and thermal conductivity as these properties affect both the driving force and vapor permeability. By modeling the coupled mass and heat transfer, we evaluate trans-membrane temperature difference and its impact on vapor transport driving force.

https://doi.org/10.1021/acs.est.2c07765
Environ. Sci. Technol. 2023, 57, 2129−2137

Last, we summarize the research needs and strategies to develop high-performance PD membranes.

THEORY

In PD, vapor transfer through the membrane is driven by the difference of partial vapor pressure between the feed−membrane interface and the distillate−membrane interface. The partial vapor pressure difference across the membrane (i.e., the driving force) is affected by applied hydraulic pressure, temperature, and feed salinity. The dependence of the saturated vapor pressure on hydraulic pressure is described by Kelvin's equation, which holds true for nanoscale radius of curvature and high pressures[27]

$$P_v(\Delta P_h, T, C) = P_v(T, C)\ \exp\left(\frac{\Delta P_h \nu_w}{RT}\right) \quad (1)$$

where ΔP_h is the hydraulic pressure difference, ν_w is the molar volume of liquid water, R is the ideal gas constant, and $P_v(T, C)$ is the saturated vapor pressure at temperature T and salinity C under ambient pressure. Specifically, the dependence of P_v on T is described by Antoine equation for pure water and the dependence of P_v on C is a colligative property of solution

$$P_v(T, C) = P_v(T)a_w(C) \quad (2)$$

where $P_v(T)$ is the saturated vapor pressure of pure water and $a_w(C)$ is the activity of water in a solution of solute concentration, C [eqs S7 and S8 for numerical forms of $P_v(T)$ and $a_w(C)$, respectively]. Since a PD membrane rejects all nonvolatile solutes, the partial vapor pressure on the distillate side simply depends on temperature following Antoine equation.

Equation 1 may be linearized when ΔP_h is small ($\ll RT/\nu_w$, which evaluates to ∼1400 bar at 25 °C). When the feed solution is sufficiently dilute, eq 2 can be reduced to Raoult's law where $a_w(C)$ is replaced by the molar fraction of water, x_w. Applying these two simplifications leads to the linearized form[14]

$$P_v(\Delta P_h, T, C) = P_v(T)\left(1 + \frac{\Delta P_h \nu_w}{RT}\right)x_w(C) \quad (3)$$

As will be shown later (as one of the key questions to be answered in this work), a significant temperature difference will never develop across the membrane. Therefore, we can apply eq 3 with the same temperature to describe the partial vapor pressure of both the feed and distillate, which leads to a simple expression to describe the transmembrane vapor pressure difference (i.e., the driving force for PD) as proposed by Lee and Karnik[14]

$$\Delta P_v(\Delta P_h, T, C_F) = \frac{P_v(T)\nu_w}{RT}(\Delta P_h - \Delta\pi(C_F)) \quad (4)$$

Equation 4 is essentially equivalent to the equation for describing water transport driving force in RO with a conversion factor. Therefore, PD behaves the same as RO at and beyond the coupon scale and that it only differs in mechanisms of mass transfer at the pore scale, which has important implications that we will further elaborate at the end of this paper. Since we have not proven the lack of transmembrane temperature difference up to this point, we will still use eqs 2 and 3 in the following analysis.

The mass and heat transfer across the vapor gap is coupled. Evaporating water molecules carry the latent heat across the membrane via convective heat transfer, and the trans-membrane temperature difference results in a reverse conductive heat transfer from the distillate to the feed. Concentration polarization (CP) occurs only in the feed side boundary layer, while temperature polarization (TP) occurs in the boundary layers of both sides of the feed and distillate (Figure 1B). The coupled mass- and heat-transfer model in PD can be described with the state-of-the-art model framework for membrane distillation with minimal modification, with the model details provided in Sections S2 and S3.[28] Such a model framework considers the resistance of vapor transport (described by the dusty-gas model) and phase change at the interfaces. Briefly, the vapor flux is proportional to the partial vapor pressure difference with a proportionality factor called the vapor permeability coefficient. The inverse of vapor permeability is the vapor transport resistance which has both interfacial resistance and transmission resistance. The calculation procedures for flux and rejection of a membrane with log−normal pore size distribution are presented in S4.

RESULTS AND DISCUSSION

Driving Force in PD. In general, the hydraulic pressure difference, ΔP_h, generates a vapor transport driving force from the feed to the distillate. Such a driving force is reduced by the feed salinity and the trans-membrane temperature difference (higher in the distillate), ΔT. Consequently, for a given feed solution, a set of conditions defined by ΔP_h and ΔT demarcate two operation regimes (Figure 1C): when ΔP_h is relatively high and ΔT is relatively low, vapor transport occurs in the forward direction (i.e., from the feed to the distillate); when ΔP_h is relatively low and ΔT is relatively high, vapor transport occurs in the reverse direction (i.e., from the distillate to the feed). The boundary of the two operation regimes in Figure 1C represents equilibrium conditions with no vapor transport driving force. For NaCl solutions of 0.6 M (representative of seawater salinity) and 0.1 M (representative of brackish water salinity),[29,30] the equilibrium ΔP_h (at 20 °C) without temperature difference is ∼27 and ∼4 bar, respectively. With a small ΔT of ∼0.9 °C, the equilibrium ΔP_h is ∼100, ∼77, and ∼73 bar for 0.6 M NaCl solution, 0.1 M NaCl solution, and pure water, respectively. For PD to be practically useful, any reverse temperature difference that develops due to heat transfer should be substantially lower than 0.1 °C. The feed salinity affects water flux via affecting the partial vapor pressure difference, that is, the driving force. For a given operating hydraulic pressure, water flux decreases with increasing feed salinity (Figure S2). According to eqs S6−S8, the feed water activity and the partial vapor pressure at the feed−membrane interface decrease with increasing NaCl molarity, which results in reduced partial vapor pressure difference across the membrane.

Nonwetting Criteria. Because of the large required ΔP_h for PD to generate a forward vapor flux (with seawater) and yet a PD membrane is porous, pore wetting is an important design consideration for developing a PD membrane. The nonwetting criterion is that ΔP_h does not exceed the liquid entry pressure (LEP) which is the minimum pressure required for a liquid to enter the membrane pores. LEP depends only on membrane and solution properties and can be calculated using eq. 5[31,32]

$$\mathrm{LEP} = -\frac{2B\gamma_L \cos\theta_0}{r} \quad (5)$$

https://doi.org/10.1021/acs.est.2c07765
Environ. Sci. Technol. 2023, 57, 2129−2137

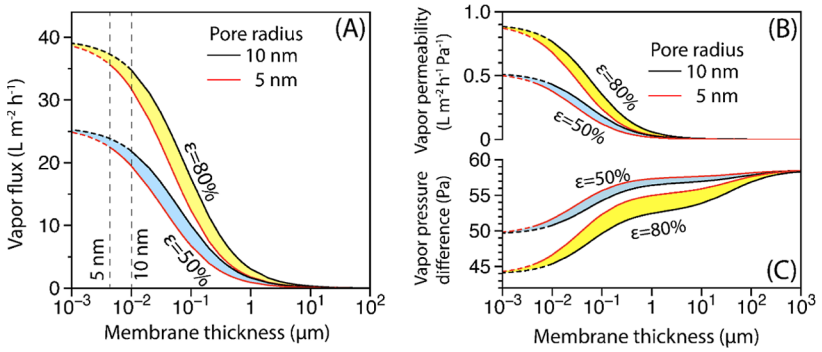

Figure 2. (A) Water flux, (B) vapor permeability, and (C) partial vapor pressure difference as a function of membrane thickness with a pore radius of 5 nm (red curves) and 10 nm (black curves) in PD for seawater desalination. The porosity is 50% (blue region) or 80% (yellow region). The applied hydraulic pressure is 60 bar, and the initial temperatures for the feed and distillate are both 20 °C. The polymer thermal conductivity is 0.16 W m^{-1} K^{-1}. The feed solution is 0.6 M NaCl (representing seawater), and the distillate is pure water. The mass-transfer coefficient of feed stream is 150 L m^{-2} h^{-1}. The dashed parts of the curves indicate ranges of membrane thickness where pore wetting is expected (i.e., thickness smaller than pore radius).

where B is a geometric factor ($0 < B < 1$ with $B = 1$ for perfect cylindrical pores), γ_L is the liquid surface tension, θ_0 is the intrinsic contact angle between the liquid and solid membrane material, and r is the radius of the largest pore. To withstand a high hydraulic pressure, the membrane should be composed of a material with low surface energy (to increase θ_0) and reduced pore radius (Figure 1D). The commercial polyvinylidene fluoride or polytetrafluoroethylene membrane with a pore radius of 0.1−1.0 μm has an LEP of only a few bars.[33,34] These membranes may be used in low-pressure PD for brackish water desalination or wastewater reuse. For seawater desalination using PD, the required LEP entails a membrane pore size of tens or even only several nanometers.

In a practical PD process, ΔP_h depends on both feed salinity and water recovery (WR). The concentration of the brine, C_B, scales with WR in PD as in RO following this relation resulting from solute mass balance[35]

$$C_B(\mathrm{WR}) = \frac{C_0}{1 - \mathrm{WR}} \tag{6}$$

where C_0 is the concentration of the feed influent. If the transmembrane temperature difference can be neglected (validity to be verified), the minimum hydraulic pressure to achieve a certain WR, $\Delta P_{h,min}(\mathrm{WR})$, can be obtained by combining eqs 1 and 2

$$\Delta P_{h,min}(\mathrm{WR}) = -\frac{RT}{\nu_W} \ln[a_w(C_B(\mathrm{WR}))] = \pi_B \tag{7}$$

where π_B is the osmotic pressure of the brine at C_B(WR) (Figure S2).

Applying the nonwetting criterion throughout the module requires $\Delta P_{h,min}$(WR) to be lower than LEP. Therefore, the pore size of a PD membrane also determines the maximum achievable WR for a given feed solution. Besides ΔP_h < LEP, an additional nonwetting criterion is that feed solution intrusion depth be less than the pore length to prevent the merging of two menisci. The maximum intrusion depth is the minimum radius of curvature and thus the pore radius. Therefore, the second nonwetting criterion demands that the hydrophobic layer thickness exceeds the pore radius.

Membrane Properties Strongly Influence Vapor Flux. Vapor flux in MD depends on both vapor permeability and driving force, which in turn depend on membrane properties including thickness, pore size, and porosity. Membrane thickness is a critical parameter because it strongly affects both water permeability and driving force (Figure 2). Commercial hydrophobic membranes used for MD typically have a thickness of 50−200 μm[36] and will yield a vapor flux lower than 0.1 L m^{-2} h^{-1} in PD (Figure 2A). These membranes can generate reasonably high flux in MD but not in PD because the driving force in MD is 1 to 2 orders of magnitudes higher than that in PD. For example, assuming that the feed solution is a 0.6 M NaCl solution and the distillate is pure water at 20 °C, heating up the feed solution to 60 °C (without considering TP) generates a vapor pressure difference of 17 kPa, contrasting the mere 0.078 kPa from pressurizing the feed solution to 70 bar. Within the range of thickness satisfying the second nonwetting criterion, vapor flux increases as the hydrophobic layer becomes thinner. Figure 2A also reveals that vapor flux is higher with a larger pore size and a higher porosity, although a larger pore size will limit the applicable hydraulic pressure. The state-of-the-art TFC-PA RO membranes have a water permeability of 1−2 L m^{-2} h^{-1} bar^{-1}. Results from Figure 2A suggest that an ultrathin (<10 nm) and highly porous (80% porosity) hydrophobic layer can yield an equivalent water permeability of above 1 L m^{-2} h^{-1} bar^{-1}, comparable to that of TFC-PA RO membranes.

Vapor permeability is higher with thinner membranes, larger pores, and/or a higher porosity (Figure 2B). With a membrane thickness that can yield a reasonable vapor flux (<100 nm according to Figure 2A), the transmission resistance against Knudsen and molecular diffusions, as well as the interfacial resistance due to liquid−vapor phase change, are both important (Figure S3). The vapor-transfer driving force, that is, the transmembrane vapor pressure difference, is strongly affected by heat transfer, including both the convective and conductive heat transfer. A thicker membrane and smaller pores both hinder vapor transport (Figure 2B) and thereby reduce forward convective heat transfer and preserve vapor transport driving force. Reducing porosity also preserves vapor transport driving force via both hindering forward convective heat transfer (by reducing vapor flux) and promoting reverse conductive heat transfer. Conductive heat transfer is enhanced with a membrane of lower porosity because the membrane matrix has a larger fraction of the more thermally conductive solid material.

https://doi.org/10.1021/acs.est.2c07765
Environ. Sci. Technol. 2023, 57, 2129−2137

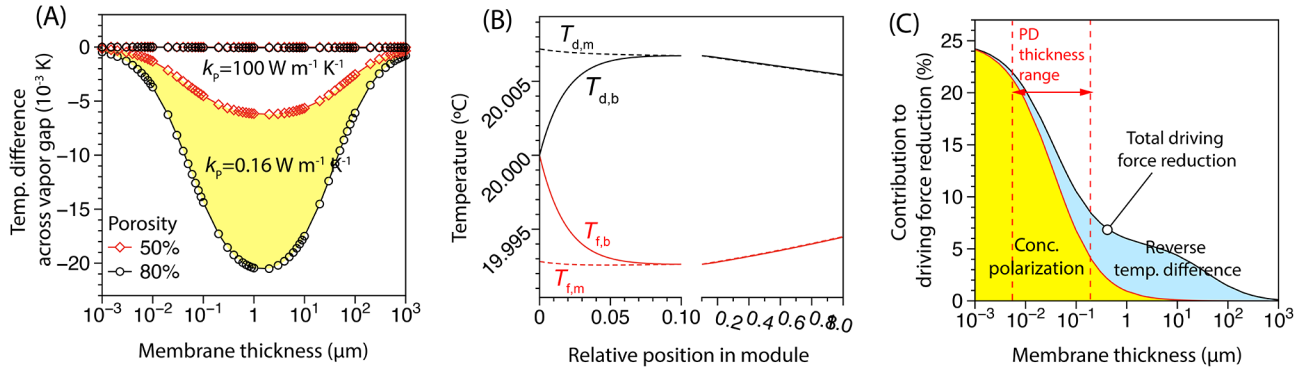

Figure 3. (A) Difference in interfacial temperatures between the feed and distillate as a function of membrane thickness for two different porosities (red diamonds for 0.5 and black circles for 0.8) and thermal conductivities of the membrane solid materials (0.16 vs 100 W m^{-1} K^{-1}). (B) Bulk temperatures of the feed ($T_{f,b}$) and the distillate ($T_{d,b}$) and the interfacial temperatures of the feed ($T_{f,m}$) and the distillate ($T_{d,m}$), as a function of the relative position in the module. The ratio of membrane area to feed flow is 50 m^2 m^{-3} h with a water recovery of 42%. (C) Contributions of CP (yellow) and reverse temperature difference (blue) to driving force reduction, i.e., the reduction of vapor pressure difference as compared to ideal vapor pressure difference if there were no CP and reverse temperature difference. The results in (B,C) are simulated using the following parameters: the pore radius is 5 nm, the porosity is 0.8, the membrane thickness is 0.1 μm, the mass-transfer coefficient is 150 L m^{-2} h^{-1}, and the heat-transfer coefficient is 3000 W m^{-2} K^{-1}.

Comparing the impacts of membrane properties on vapor permeability (Figure 2B) and vapor pressure difference (Figure 2C) to that on vapor flux (Figure 2A) suggests that vapor permeability plays a dominant role in determining the impacts of membrane properties on vapor flux. Specifically, vapor permeability (Figure 2B) varies more significantly than transmembrane vapor pressure difference (Figure 2C) with the same changes in membrane properties. Therefore, the general criteria for designing a PD membrane with high vapor flux are largely the same as designing a membrane with a high vapor permeability, that is, the membrane should be highly porous and thin and have a large pore size within the permissible limit of the nonwetting criteria.

Convective Heat Transfer Does NOT Kill PD. As previously discussed, a major concern regarding the practical viability of PD is the development of a reverse temperature difference (higher in the distillate), ΔT, due to convective heat transfer (Figure 1A). However, our analysis of the coupled mass and heat transfer in PD shows that ΔT is very small in all practical scenarios. With a thermal conductivity of 0.16 W m^{-1} K^{-1}, which is representative of polymer materials,[37] the maximum ΔT is no more than 0.02 °C when the porosity is 0.8 (Figure 3A). At the same membrane thickness, a lower porosity results in a smaller ΔT because of both lower thermal conductivity of air (0.025 W m^{-1} K^{-1}) as compared to polymer and the reduced convective heat transfer due to a lower vapor flux.

Interestingly, ΔT reaches a maximum at a membrane thickness of several micrometers regardless of porosity (Figure 3A), which can be explained by the qualitatively similar dependence of vapor flux and conductive heat transfer on membrane thickness. For a thick membrane with which reverse conductive heat transfer is less efficient, the vapor flux is small (Figure 2A) and thus the forward convective heat transfer is also limited. With an ultrathin membrane which generates a high vapor flux, the reverse conductive heat transfer is very efficient according to the Fourier law, which prevents the build-up of a large ΔT. Therefore, for an ideal PD membrane that is thin enough to sustain a high vapor flux, driving force elimination due to a reverse temperature difference is negligible due to the highly efficient reverse conductive heat transfer. Increasing the thermal conductivity of the membrane material (e.g., using carbonaceous materials) helps further reducing ΔT to practically 0 (Figure 3A), which is nonetheless unnecessary.

Since an ultrathin hydrophobic layer (<100 nm) lacks the necessary mechanical strength, a robust hydrophilic support is required to construct a thin-film composite membrane to withstand a high hydraulic pressure. Such a hydrophilic support faces the distillate and creates a hydrodynamically stagnant layer that hinders heat transfer to the bulk distillate outside the support layer. We show that the hydrophilic support in a practical membrane has no observable impact of vapor flux (Figure S4) because the reverse conductive transmembrane heat transfer is sufficiently fast and dominates the heat dissipation, dwarfing the contribution from forward heat transfer to the bulk distillate in the thick support.

Extending the mass- and heat-transfer analysis from a membrane coupon to a module further confirms that the build-up of a reverse temperature difference is negligible (Figure 3B). With the specific conditions used for simulating Figure 3B, the transmembrane temperature difference, whether defined based on interfacial temperatures or bulk temperatures, is less than 0.02 °C. The effect of TP, which creates a difference between the bulk and interfacial temperatures, is slightly stronger near the module entrance and vanishes completely at around ~10% into the module. Even though the heat-transfer coefficient in the boundary layer changes with the spatially varying hydrodynamic condition along a membrane module, here we use the approximation of a constant heat-transfer coefficient throughout the module for a simplified analysis. This simplification can be justified as we show that changing the heat-transfer coefficient at the coupon level (500 vs 3000 W m^{-2} K^{-1}) has no observable impact on vapor flux (Figure S5). The lack of dependence of vapor flux on the heat-transfer coefficient is the result of the practically negligible temperature transmembrane gradient, as shown in Figure 3A,B.

While the axial distributions of bulk and interfacial temperatures can be explained by the coupled mass and heat transfer along the module, the detailed profiles are unimportant as the transmembrane temperature difference remains extremely small along the module. For a given feed

https://doi.org/10.1021/acs.est.2c07765
Environ. Sci. Technol. 2023, 57, 2129−2137

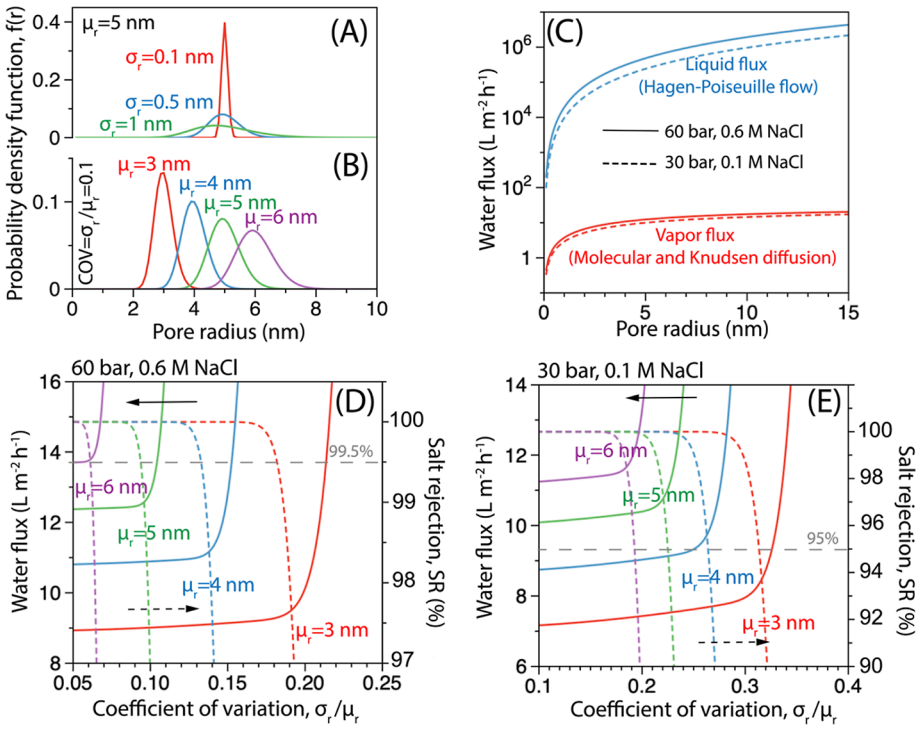

Figure 4. (A) Probability density function as a function of pore radius for log−normal pore size distributions with a mean radius of μ_r and different standard deviations, σ_r. (B) Probability density function of log−normal pore size distribution with different mean radii and a constant coefficient of variation (COV, defined as σ_r/μ_r). (C) Liquid flux through wetted pores and vapor flux through nonwetted pores as functions of pore radius for two scenarios, seawater desalination (solid curves) and brackish water desalination (dashed curves). The liquid flux is calculated using Hagen−Poiseuille equation, whereas the vapor flux is modeled using the theory of PD. (D,E) Overall water flux (solid lines) and salt rejection (dashed lines) of partially wetted membranes with log−normal pore size distributions for two scenarios, seawater desalination (D) and brackish water desalination (E). For seawater desalination, the feed solution is 0.6 M NaCl and the hydraulic pressure is 60 bar. For brackish water desalination, the feed solution is 0.1 M NaCl and the hydraulic pressure is 30 bar. Other parameters used in simulating C−E are summarized as following: the membrane thickness is 100 nm and the porosity is 0.8. The initial temperatures for the feed and distillate are both 20 °C. The polymer thermal conductivity is 0.16 W m^{-1} K^{-1}. The mass-transfer coefficient of feed stream is 150 L m^{-2} h^{-1}.

solution and applied pressure, water recovery increases with larger membrane area (Figure S6), but the maximum achievable water recovery is essentially limited by the applied hydraulic pressure according to eq 7 (Figure S2), which is identical to the behavior of RO.

Our analysis also shows that reverse temperature difference only has an observable impact on driving force reduction (~5%) only when the membranes have a relatively thick hydrophobic layer (Figure 3C). However, when the hydrophobic layer thickness falls within the range that is required to yield a reasonable vapor flux (<100 nm), the impact of reverse temperature difference becomes negligible compared to CP. A thinner hydrophobic layer promotes both vapor transport and conductive heat transfer, with the former leading to more severe CP and the latter resulting in a smaller reverse temperature difference. We note that CP is not unique to PD but is universal in all membrane-based processes (e.g., RO).

Need for Membranes with Highly Uniform Pore Size Distributions. The analysis of wetting criteria and of mass and heat transfer in PD is developed based on the ideal assumption of a perfectly uniform pore size distribution. With this assumption, the pore can either be wetted or be nonwetted under a given hydraulic pressure. However, the heterogeneity in pore size distribution in real membranes has substantial impacts on membrane design, mainly through the impact of wetted pore on water flux and SR. If we assume a log−normal distribution to simulate the distribution of membrane pore size (a commonly adopted distribution)[38−40] and allow a portion of the pores to be wetted, we can evaluate the overall water flux and SR at a given hydraulic pressure.

Specifically, the PD membrane is conceptualized as an array of cylindrical pores with a porosity (ε) and tortuosity (τ), with the two parameters related by the Bruggeman correlation (i.e., $\tau = \varepsilon^{-0.5}$).[41] The pore size distribution, $f(r)$, follows a log−normal distribution with a mean pore size of μ_r and a standard variation of σ_r (eqs S25−S27). Example pore size distributions are illustrated in Figure 4A with a constant μ_r and a series of σ_r and in Figure 4B with a constant σ_r and a series of μ_r. For a given hydraulic pressure, ΔP_h, the nonwetting criterion ($\Delta P_h \leq$ LEP) and eq 5 suggest that there exists a critical pore size, $r^*(\Delta P_h)$, for a given membrane material. For pores with a radius smaller than $r^*(\Delta P_h)$, water transports as vapor according to the mechanism of PD and pore-level SR is 100%; for pores with a radius larger than $r^*(\Delta P_h)$, water transports due to pressure-driven liquid flow (eq S28) and the pore-level SR is zero. For a membrane with an intrinsic contact angle of 110°, the critical radii are 8.3 and 16.6 nm for ΔP_h of 60 and 30 bar, respectively.

For a given pair of $f(r)$ and ΔP_h, the overall water flux, J_w, can be evaluated using the follow equation

https://doi.org/10.1021/acs.est.2c07765
Environ. Sci. Technol. 2023, 57, 2129−2137

$$J_w = \frac{\int_0^{r*(\Delta P_h)} J_v(r) r^2 f(r)\,dr + \int_{r*(\Delta P_h)}^{\infty} J_l(r) r^2 f(r)\,dr}{\int_0^{\infty} r^2 f(r)\,dr} \quad (8)$$

where $J_v(r)$ is the porosity-corrected pore-level vapor flux for pore with a radius, r (eq S9), and $J_l(r)$ is the porosity-corrected pore-level liquid flux for pore with a radius, r (eq S29) following Hagen−Poiseuille equation. With a pressure at tens of bar, $J_l(r)$ is 3−6 orders of magnitude higher than $J_v(r)$, depending on pore radius (Figure 4C), which suggests that $J_l(r)$ can dominate J_w with a tiny fraction of wetted pores. The SR is given by

$$SR = 1 - \frac{1}{J_w} \frac{\int_{r*(\Delta P_h)}^{\infty} J_l(r) r^2 f(r)\,dr}{\int_0^{\infty} r^2 f(r)\,dr} \quad (9)$$

We note that SR is independent of the feed concentration.

The simulated J_w and SR with different mean radii (μ_r) and standard variations (σ_r) show that the tolerable σ_r is strongly dependent on the μ_r (Figure 4D,E). Setting 99.5% as acceptable SR for seawater desalination, the tolerable σ_r for a distribution with μ_r = 6 nm is ∼0.3 nm, corresponding to a COV of ∼0.05 (Figure 4D), which requires the membrane to be highly uniform. Reducing μ_r to 3 nm will increase the tolerable σ_r to ∼0.6 nm and a corresponding COV of ∼0.2. For brackish water desalination operated at a lower pressure (30 bar) with an SR of 95%, the tolerable σ_r and the corresponding COV are substantially higher, especially for relatively large pores (e.g., μ_r = 6 nm). However, the acceptable COV, even for the membrane with a μ_r of 3 nm, is only slightly above 0.3, which is still very small compared to that of commercial polymeric membranes. Typical COV of an ultrafiltration membrane (μ_r is a few nm) is ∼0.5, whereas the typical COV of a microfiltration used in membrane distillation is even higher.[40,42]

PERSPECTIVE

PD is a relatively new concept in desalination. In theory, PD should have a similar energy efficiency of RO, but it also has several additional intrinsic advantages, including the high rejection of small neutral solutes, not being constraint by the permeability−selectivity tradeoff, and the compatibility with chlorination for biofouling control. Our analysis shows that, despite the large amount of latent heat carried by vapor flux from the feed to the distillate and the very high sensitivity of partial vapor pressure to temperature, heat accumulation in the distillate and the consequent driving force elimination are NOT a practical challenge due to the very efficient reverse conductive heat transfer when the PD membrane is sufficiently thin to provide the necessary vapor permeability. In other words, PD is practically viable from a process perspective.

We note that there may be additional contribution from water−membrane interaction to the vapor transport kinetics and that the current model framework (based on the dusty-gas model) may not accurately predict vapor flux through nanoscale pores.[43] Nonetheless, we still used this model framework in the current study because (1) no well-established model exists that can accurately account for the nanopore effects absent in the current MD model and (2) imperfect prediction of flux will not affect the validity of two main conclusions of our analysis regarding the lack of reverse temperature difference and the impact of pore size distribution on pore wetting and its consequences. Moving forward, we expect that the improved mass-transfer model will be developed for PD and MD with membranes containing nanoscale pores, especially when more fundamental understanding of how nanopores affect interfacial and transmission resistances becomes available.

The macroscopic (coupon scale and beyond) working principle of PD resembles that of RO. Therefore, the transition from RO to PD only requires repurposing existing RO plants by replacing RO modules with PD modules with little modification of other auxiliary components (e.g., pumps and energy recovery device). The macroscopic equivalence between RO and PD also means that our rich knowledge of RO behaviors at the coupon and module scale is directly applicable to understanding PD. Specifically, the influence of feed salinity, operating pressure, and water recovery on water flux and energy consumption, which has been well understood in RO, still applies equally to PD. For example, the state-of-the-art RO process for seawater desalination consumes around 2−3 kW h to produce one cubic meter of freshwater, and we expect that PD will have very similar energy consumption. Therefore, the module-scale process control and optimization for PD can also adopt those that have been developed for RO with minor modifications and the future development of PD is expected to heavily rely on advances in membrane materials.

The ideal PD membrane for seawater or brackish desalination should be a thin-film composite membrane with a hydrophilic support to provide mechanical strength and an ultrathin, porous hydrophobic layer (tens−hundreds of nanometers thick) with uniform nanoscale pores made of low-surface-energy materials. Membrane material with high thermal conductivity has quantitatively negligible benefits. Without considering heterogeneity in pore size distribution, the pore size of an ideal PD membrane can be tens of nanometers to provide a high vapor permeability while imparting a sufficient LEP. With more realistic heterogeneous pore size distributions, a mean pore size of a few nanometers may still be insufficient given the typical degree of pore size heterogeneity in commercial polymer membranes. Therefore, substantial advancement in fabricating hydrophobic membranes with highly uniform, nanometer-sized pores is required to push the field of PD toward practical applications. Ideally, these membranes should also be easy and cheap to fabricate in large scale. All these requirements create a unique opportunity for the material scientists in the membrane community to contribute to the next potential revolution in desalination.

ASSOCIATED CONTENT

Supporting Information

The Supporting Information is available free of charge at https://pubs.acs.org/doi/10.1021/acs.est.2c07765.

Details on dependence of chemical potential on pressure; calculation of saturated vapor pressure; mass- and heat-transfer model for PD; and dependence of flux and rejection on pore size distribution (PDF)

AUTHOR INFORMATION

Corresponding Author

Shihong Lin − *Department of Civil and Environmental Engineering and Department of Chemical and Bimolecular Engineering, Vanderbilt University, Nashville, Tennessee*

https://doi.org/10.1021/acs.est.2c07765
Environ. Sci. Technol. 2023, 57, 2129−2137

37235-1831, United States; orcid.org/0000-0001-9832-9127; Email: shihing.lin@vanderbilt.edu

Authors

Weifan Liu − *Department of Civil and Environmental Engineering, Vanderbilt University, Nashville, Tennessee 37235-1831, United States*

Ruoyu Wang − *Department of Civil and Environmental Engineering, Vanderbilt University, Nashville, Tennessee 37235-1831, United States*

Anthony P. Straub − *Department of Civil, Environmental and Architectural Engineering, University of Colorado Boulder, Boulder, Colorado 80309-0428, United States;* orcid.org/0000-0001-7233-6839

Complete contact information is available at: https://pubs.acs.org/10.1021/acs.est.2c07765

Notes

The authors declare no competing financial interest.

■ ACKNOWLEDGMENTS

W.L., R.W., and S.L. acknowledges support from the National Science Foundation (1903685 and 2017998), the Water Research Foundation (Paul L Busch Award), and the US-Israel Binational Agricultural Research and Development (IS-5209-19). A.P.S. acknowledges support from the Bureau of Reclamation, Department of Interior, via DWPR Agreement R22AC00425 and the NSF Industry/University Cooperative Research Center for Membrane Science, Engineering and Technology (MAST) at the University of Colorado Boulder (UCB, award number, IIP 1624602).

■ REFERENCES

(1) Shannon, M. A.; Bohn, P. W.; Elimelech, M.; Georgiadis, J. G.; Mariñas, B. J.; Mayes, A. M. Science and technology for water purification in the coming decades. *Nature* **2008**, *452*, 301−310.

(2) Urban, J. J. Emerging Scientific and Engineering Opportunities within the Water-Energy Nexus. *Joule* **2017**, *1*, 665−688.

(3) Elimelech, M.; Phillip, W. A. The Future of Seawater Desalination: Energy, Technology, and the Environment. *Science* **2011**, *333*, 712−717.

(4) Biesheuvel, P. M.; Zhang, L.; Gasquet, P.; Blankert, B.; Elimelech, M.; van der Meer, W. G. J. Ion Selectivity in Brackish Water Desalination by Reverse Osmosis: Theory, Measurements, and Implications. *Environ. Sci. Technol. Lett.* **2020**, *7*, 42−47.

(5) Greenlee, L. F.; Lawler, D. F.; Freeman, B. D.; Marrot, B.; Moulin, P. Reverse osmosis desalination: Water sources, technology, and today's challenges. *Water Res.* **2009**, *43*, 2317−2348.

(6) Werber, J. R.; Deshmukh, A.; Elimelech, M. The Critical Need for Increased Selectivity, Not Increased Water Permeability, for Desalination Membranes. *Environ. Sci. Technol. Lett.* **2016**, *3*, 112−120.

(7) Hyung, H.; Kim, J.-H. A mechanistic study on boron rejection by sea water reverse osmosis membranes. *J. Membr. Sci.* **2006**, *286*, 269−278.

(8) Miyashita, Y.; Park, S. H.; Hyung, H.; Huang, C. H.; Kim, J. H. Removal of N-Nitrosamines and Their Precursors by Nanofiltration and Reverse Osmosis Membranes. *J. Environ. Eng.* **2009**, *135*, 788−795.

(9) Powell, J.; Luh, J.; Coronell, O. Bulk Chlorine Uptake by Polyamide Active Layers of Thin-Film Composite Membranes upon Exposure to Free Chlorine-Kinetics, Mechanisms, and Modeling. *Environ. Sci. Technol.* **2014**, *48*, 2741−2749.

(10) Stolov, M.; Freger, V. Degradation of Polyamide Membranes Exposed to Chlorine: An Impedance Spectroscopy Study. *Environ. Sci. Technol.* **2019**, *53*, 2618−2625.

(11) Park, H. B.; Kamcev, J.; Robeson, L. M.; Elimelech, M.; Freeman, B. D. Maximizing the right stuff: The trade-off between membrane permeability and selectivity. *Science* **2017**, *356*, No. eaab0530.

(12) Geise, G. M.; Park, H. B.; Sagle, A. C.; Freeman, B. D.; McGrath, J. E. Water permeability and water/salt selectivity tradeoff in polymers for desalination. *J. Membr. Sci.* **2011**, *369*, 130−138.

(13) Yang, Z.; Guo, H.; Tang, C. Y. Y. The upper bound of thin-film composite (TFC) polyamide membranes for desalination. *J. Membr. Sci.* **2019**, *590*, 117297.

(14) Lee, J.; Karnik, R. Desalination-of water by vapor-phase transport through hydrophobic nanopores. *J. Appl. Phys.* **2010**, *108*, 044315.

(15) Deshmukh, A.; Elimelech, M. Understanding the impact of membrane properties and transport phenomena on the energetic performance of membrane distillation desalination. *J. Membr. Sci.* **2017**, *539*, 458−474.

(16) Mulder, M.; Mulder, J.*Basic Principles of Membrane Technology*; Springer Science & Business Media, 1996.

(17) Wijmans, J. G.; Baker, R. W. The Solution-Diffusion Model—a Review. *J. Membr. Sci.* **1995**, *107*, 1−21.

(18) Lee, S.; Straub, A. P. Opportunities for high productivity and selectivity desalination via osmotic distillation with improved membrane design. *J. Membr. Sci.* **2020**, *611*, 118309.

(19) Qtaishat, M. R.; Obaid, M.; Matsuura, T.; Al-Samhouri, A.; Lee, J. G.; Soukane, S.; Ghaffour, N. Desalination at ambient temperature and pressure by a novel class of biporous anisotropic membrane. *Sci. Rep.* **2022**, *12*, 13564.

(20) Asatekin, A.; Gleason, K. K. Polymeric Nanopore Membranes for Hydrophobicity-Based Separations by Conformal Initiated Chemical Vapor Deposition. *Nano Lett.* **2011**, *11*, 677−686.

(21) Wang, Y. T.; Han, M. Y.; Liu, L.; Yao, J. M.; Han, L. Beneficial CNT Intermediate Layer for Membrane Fluorination toward Robust Superhydrophobicity and Wetting Resistance in Membrane Distillation. *ACS Appl. Mater. Interfaces* **2020**, *12*, 20942−20954.

(22) Lee, J.; Laoui, T.; Karnik, R. Nanofluidic transport governed by the liquid/vapour interface. *Nat. Nanotechnol.* **2014**, *9*, 317−323.

(23) Chen, W.; Chen, S. Y.; Liang, T. F.; Zhang, Q.; Fan, Z. L.; Yin, H.; Huang, K. W.; Zhang, X. X.; Lai, Z. P.; Sheng, P. High-flux water desalination with interfacial salt sieving effect in nanoporous carbon composite membranes. *Nat. Nanotechnol.* **2018**, *13*, 345−350.

(24) Gong, D. A.; Yin, Y. C.; Chen, H. L.; Guo, B.; Wu, P.; Wang, Y.; Yang, Y.; Li, Z. K.; He, Y.; Zeng, G. F. Interfacial Ions Sieving for Ultrafast and Complete Desalination through 2D Nanochannel Defined Graphene Composite Membranes. *ACS Nano* **2021**, *15*, 9871−9881.

(25) Lin, S. H.; Yip, N. Y.; Elimelech, M. Direct contact membrane distillation with heat recovery: Thermodynamic insights from module scale modeling. *J. Membr. Sci.* **2014**, *453*, 498−515.

(26) Straub, A. P.; Yip, N. Y.; Lin, S. H.; Lee, J.; Elimelech, M. Harvesting low-grade heat energy using thermo-osmotic vapour transport through nanoporous membranes. *Nat. Energy* **2016**, *1*, 16090.

(27) Adamson, A. W.; Gast, A. P.*Physical Chemistry of Surfaces*; Interscience Publishers: New York, 1997; Vol. *150*.

(28) Deshmukh, A.; Lee, J. Membrane desalination performance governed by molecular reflection at the liquid-vapor interface. *Int. J. Heat Mass Transfer* **2019**, *140*, 1006−1022.

(29) Lim, Y. J.; Goh, K.; Kurihara, M.; Wang, R. Seawater desalination by reverse osmosis: Current development and future challenges in membrane fabrication ? A review. *J. Membr. Sci.* **2021**, *629*, 119292.

(30) Patel, S. K.; Biesheuvel, P. M.; Elimelech, M. Energy Consumption of Brackish Water Desalination: Identifying the Sweet Spots for Electrodialysis and Reverse Osmosis. *ACS ES&T Engg* **2021**, *1*, 851−864.

(31) Franken, A. C. M.; Nolten, J. A. M.; Mulder, M. H. V.; Bargeman, D.; Smolders, C. A. Wetting Criteria for the Applicability of Membrane Distillation. *J. Membr. Sci.* **1987**, *33*, 315−328.

(32) García-Payo, M. C.; Izquierdo-Gil, M. A.; Fernández-Pineda, C. Wetting study of hydrophobic membranes via liquid entry pressure measurements with aqueous alcohol solutions. *J. Colloid Interface Sci.* **2000**, *230*, 420−431.
(33) Wang, W.; Du, X. W.; Vahabi, H.; Zhao, S.; Yin, Y. M.; Kota, A. K.; Tong, T. Z. Trade-off in membrane distillation with monolithic omniphobic membranes. *Nat. Commun.* **2019**, *10*, 3220.
(34) Feng, D. J.; Chen, Y. M. L.; Wang, Z. X.; Lin, S. H. Janus Membrane with a Dense Hydrophilic Surface Layer for Robust Fouling and Wetting Resistance in Membrane Distillation: New Insights into Wetting Resistance. *Environ. Sci. Technol.* **2021**, *55*, 14156−14164.
(35) Lin, S. H. Energy Efficiency of Desalination: Fundamental Insights from Intuitive Interpretation. *Environ. Sci. Technol.* **2020**, *54*, 76−84.
(36) Qasim, M.; Ul Samad, I.; Darwish, N. A.; Hilal, N. Comprehensive review of membrane design and synthesis for membrane distillation. *Desalination* **2021**, *518*, 115168.
(37) Phattaranawik, J.; Jiraratananon, R.; Fane, A. G. Heat transport and membrane distillation coefficients in direct contact membrane distillation. *J. Membr. Sci.* **2003**, *212*, 177−193.
(38) Zydney, A. L.; Aimar, P.; Meireles, M.; Pimbley, J. M.; Belfort, G. Use of the Log-Normal Probability Density-Function to Analyze Membrane Pore-Size Distributions - Functional Forms and Discrepancies. *J. Membr. Sci.* **1994**, *91*, 293−298.
(39) Bowen, W. R.; Welfoot, J. S. Modelling of membrane nanofiltration—pore size distribution effects. *Chem. Eng. Sci.* **2002**, *57*, 1393−1407.
(40) Phattaranawik, J.; Jiraratananon, R.; Fane, A. G. Effect of pore size distribution and air flux on mass transport in direct contact membrane distillation. *J. Membr. Sci.* **2003**, *215*, 75−85.
(41) Tjaden, B.; Cooper, S. J.; Brett, D. J. L.; Kramer, D.; Shearing, P. R. On the origin and application of the Bruggeman correlation for analysing transport phenomena in electrochemical systems. *Curr. Opin. Chem. Eng.* **2016**, *12*, 44−51.
(42) Wickramasinghe, S. R.; Bower, S. E.; Chen, Z.; Mukherjee, A.; Husson, S. M. Relating the pore size distribution of ultrafiltration membranes to dextran rejection. *J. Membr. Sci.* **2009**, *340*, 1−8.
(43) Fan, J.; Wu, H.; Wang, F. Evaporation-driven liquid flow through nanochannels. *Phys. Fluids* **2020**, *32*, 012001.

https://doi.org/10.1021/acs.est.2c07765
Environ. Sci. Technol. 2023, 57, 2129−2137